Density Functional Theory of Water−Gas Shift Reaction on Molybdenum Carbide

Hiroyuki Tominaga and Masatoshi Nagai*

Graduate School of Bio-applications and Systems Engineering, Tokyo University of Agriculture and Technology, 2-24 Nakamachi, Koganei, Tokyo 184-8588, Japan

Received: July 7, 2005; In Final Form: August 31, 2005

The density functional theory (DFT) of the water−gas shift (WGS) reaction over molybdenum carbide was studied with the aim of understanding the dissociation of H_2O, the OH group, and CO to determine on what sections of molybdenum carbide CO_2 and H_2 formed and whether they played a role in the reaction. The energy diagram of each elementary step, the reaction of the hydrogen and oxygen atoms with CO, and the transition state for this elementary step were also studied. The IR spectra of the CO adsorption was experimentally analyzed for the identification of several candidates of the CO adsorption modes. The adsorptions of the threefold Mo site (a) with and (b) without the underlying C atom of the second layer have the second and highest adsorption energies of −281.59 and −321.00 kJ/mol, respectively. The IR data showed that the bands at 1626 cm^{-1} from the IR experiments are (a) the nearest adsorption of the threefold Mo site with the underlying C atom at the calculated/corrected band of 1621 cm^{-1}. The calculated/corrected threefold adsorption (b) had the highest adsorption energy but exhibited an IR band at 1147 cm^{-1} which was not observed in the experimental data. The C−O bond length increased to 1.49 from 1.36 after the H_2O adsorption (b), suggesting the dissociation of C−O after the H_2O coadsorption. The WGS reaction on the β-Mo_2C(001) slab carbide was calculated and took place as follows: H_2O was dissociated into OH and H on the Mo_2C surface and the OH subsequently dissociated into H and O atoms. CO approached the O atom to form CO_2.

Introduction

The water−gas shift reaction has been studied as a CO removal technology of reformed fuels for application to fuel cells. The Cu−Zn catalysts are commercially used at the present time for the WGS reaction at low temperature[1−6] in large-scale operations and are not applicable for many fuel-cell applications due to the fact that they are sensitive to the start-up/shut-down cycles and may be pyrophoric.[7,8] The substituted metals of Cu/ZnO are being evaluated for various transition metal oxides. The molybdenum-containing catalysts have been studied for the WGS reaction, for example, potassium-promoted $NiMo/Al_2O_3$,[9] $CoMo/Al_2O_3$,[10−12] and Mo/Al_2O_3[13] catalysts are reported to be highly active for the WGS reaction. Hou et al.[14] and Łaniecki et al.[15] studied the catalytic species of the Mo sulfide-based catalyst in the presence of hydrogen sulfide and proposed a redox cycle with Mo^{5+} as the active species for the WGS reaction. For Mo carbides, Patt et al. reported a high WGS activity with good durability for the Mo carbide which has an active site density of more than 25% vs that of the Cu−Zn catalyst.[16] The catalysts with a highly active density imply a high filling probability in a compact reactor for the WGS. Moon and Ryu recently reported that the molybdenum carbide catalyst showed an activity and stability for the WGS reaction higher than the commercial low-temperature Cu−Zn catalyst.[17] Thus, the Mo carbide catalyst would have a bright prospect for use as an alternative catalyst to replace Cu−Zn catalysts for the WGS reaction under unstable oxidized operating conditions.

Although the WGS reaction involves only four small molecules, the reaction mechanism is quite complex.[3] There are generally two reaction mechanisms proposed in the literature for the WGS reaction, that is, the associative and redox mechanisms. In the first one, a formate species is formed from the surface CO and OH groups and then decomposes forming CO_2 and H_2.[4,18−20] The second one consists of a surface oxidation, $H_2O + * \rightleftarrows H_2 + O^*$ (* designates an adsorption site), followed by a surface reduction, $CO + O^* \rightleftarrows CO_2 + *$.[5,6,21−23] A more complete statement of the mechanism would separate the dissociation of water into the formation of H* and OH* and the subsequent dissociation into H* and O*. Less information, however, is available for the dissociation of OH* to H* and O* and whether the attack is CO* to O* or O* to CO*. Experimental studies are difficult because of the visible presence of the O* and H* and the attack of CO* to O* or of O* to CO* on Mo carbide, thereby obscuring information about the behavior of the adsorbed CO and OH.

Theoretical studies are challenging for the individual steps during the WGS reaction and the interaction of an adsorbed species (i.e., CO, H, O, OH, and H_2O) with the β-Mo_2C(001). There are very few reports of DFT calculations for the WGS reaction over Cu slabs to the best of our knowledge. The promotion of the WGS reaction by preadsorbed oxygen on a Cu cluster[24] and by water on Pt(111)[25] surfaces was studied by DFT, as well as the calculation of the H_2O dissociation and the reaction of the adsorbed CO and adsorbed OH on Pt and the mixed Pt metal cluster.[25,26] The DFT calculation for the Mo carbides has been performed for the geometry, stability, and properties of the Mo_8C_{12} cluster,[27,28] the adsorption of CO on Mo carbide[29] and sulfide,[30,31] and the desulfurization on the α-Mo_2C cluster.[32] In this study, we perform a periodic, self-consistent, gradient-corrected DFT investigation of the WGS reaction on a β-Mo_2C(001) slab. This reaction pathway involves the adsorption of CO, decomposition of H_2O, and the subsequent reaction of the decomposed H_2O with CO. The energy diagram

* To whom correspondence should be addressed. E-mail: mnagai@cc.tuat.ac.jp.

10.1021/jp053706u CCC: $30.25
Published on Web 10/01/2005

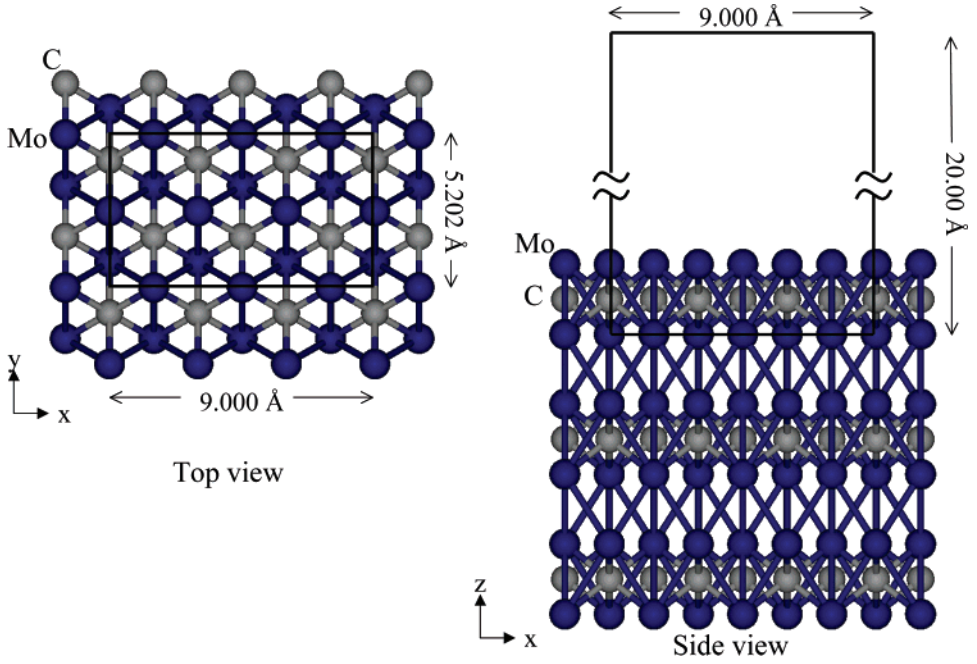

Figure 1. Schematic top and side views of the β-Mo_2C(001) slab. The Mo and C atoms are denoted by dark and gray spheres, respectively. The rectangular area indicates the supercell employed in the study, and each layer contains 12 Mo and 6 C atoms. Because, in some cases, the adsorption of carbon monoxide occurs at one Mo/C atom on the top layer, notations a, b, c, and d are used to distinguish the Mo/C atoms (also see Figure 3).

of each elementary step, the reaction of hydrogen and oxygen atoms with CO, and the transition state for this elementary step are studied. Experimentally, we studied the IR spectra of the CO adsorption for the identification of several candidates for the adsorption modes of CO. Finally, we discuss the WGS reaction mechanism and the possible role of the surface structure and surface hydrogen and oxygen of water.

Experimental/Methods Section

Catalyst Preparation. A carbided 11.6% Mo/Al_2O_3 catalyst was prepared. γ-Alumina (AL0-4 CSJ, reference) was added to an aqueous solution of ammonium paramolybdate, and the solution was boiled while being stirred. After the solid product was oxidized in dry air at 623 K for 2 h and then cooled to 573 K, the 11.6% MoO_3/Al_2O_3 was treated with 20% CH_4/H_2 at the rate of 4 L/h from 573 to 973 K at the rate of 60 K/h and then held at 973 K for 3 h. After the carbiding treatment, the catalyst was cooled to room temperature in flowing 20% CH_4/H_2.

Infrared Spectroscopy. The diffuse reflection IR spectroscopy cell used in this study allows the collection of in situ IR spectra. The carbided catalyst was not exposed to air during the procedure from the catalyst pretreatment to the IR measurement. The microreactor was transferred to a glovebox in which the atmosphere was exchanged five times with argon (99.9999%) and then filled with argon. The catalyst was removed from the microreactor in the glovebox, placed in a holder, and loaded into the IR cell of a high-temperature reaction chamber. The IR cell was placed in the IR spectrometer (Nicolet Series FTIR 750) equipped with a MCT detector. All the IR spectra were collected in the absorbance mode using 64 scans with a resolution of 4 cm^{-1}. The spectra for the CO adsorbed on the powdered sample were displayed as the ratio $-\log(R/R_0)$ where R and R_0 are the reflectance values corresponding to the sample and reference single beam spectra, respectively. The reference spectra were collected at 423 K and atmospheric pressure and at 300 K and 15 mL/min, and an IR spectrum was obtained. These spectra were used to check the reversibility of the changes in the spectra caused by changes in the sample temperature for the 11.6% Mo/Al_2O_3 catalyst.

DFT Calculations. Self-consistent, gradient-corrected, periodic DFT calculations were performed using CPMD.[33] The Perdew−Burke−Ernzerhof[34] functional was used within the generalized gradient approximation to describe the exchange and correlation effects. The Fritz-Haber-Institute pseudopotential[35] was used for all the ions. For the plane wave set, the cutoff energy was 50 Ry. The surface Brilouin zone sampling restricted to the Γ point was selected for our calculations. The convergence criteria for the energy calculation and structure optimization were set to a SCF tolerance of 1.0×10^{-7} and maximum force tolerance of 5×10^{-4}. The initial transition state structure was calculated by the synchronous transit-guided quasi-Newton method and then optimized by the partitioned rational function optimizer with a quasi-Newton method. We calculated the harmonic frequencies by finite differences of the first derivatives by a linear response to the ionic displacements.

The structures of the bulk β-Mo_2C(001) surface and selected slab are shown in Figure 1. The periodically repeated orthorhombic supercell (9.000 Å × 5.202 Å × 20.00 Å) was used. Each slab included three atomic layers with alternating layers of Mo and C; thus, the top overlayer contains six Mo atoms, the second layer six C atoms, and the third layer six Mo atoms. ViewerLite 5.0 (Accelrys, Inc.) was used to visualize the results of the computer graphics calculations. The bond length and wavenumber of C−O were calculated to be 1.14 Å and 2102 cm^{-1}, respectively, based on the CPMD calculations of C−O under these conditions. The C−O bond length was in good agreement with the experimental value of 1.13 Å,[36] and our experimental result was 2112 cm^{-1}, corresponding to the relative errors of 0.88 and 0.47% both within 1%, which suggested good reliability. The lattice constant of β-Mo_2C was calculated to be $a = b = 3.083$ Å and $c = 4.510$ Å, which was in good agreement with the reference of $a = b = 3.00$ Å and $c = 4.73$ Å (JCPDS card, $2\theta = 34.36$, 39.38, and 61.53°) at relative errors of 2.77 and 4.65%. The relative error of the cell volume was calculated to be 0.698%, thus within 1%. Because the lattice

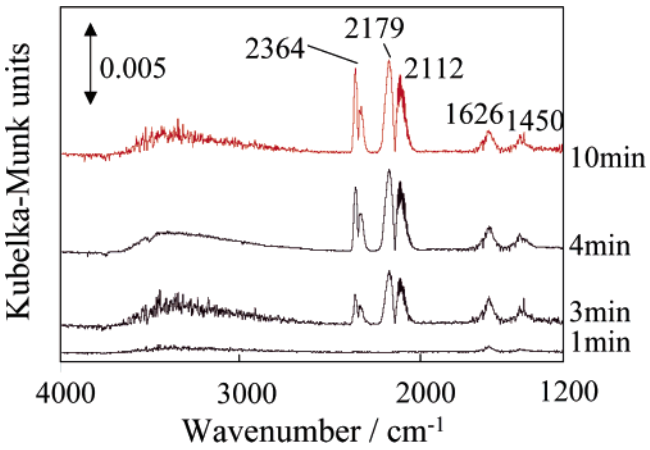

Figure 2. IR spectra for CO adsorption on 11.6% Mo/Al_2O_3 carbided at 973 K.

constant was calculated on the basis of the variation in the cell volume, this result was reliable for the calculation using CPMD.

Results and Discussion

IR Experimental Studies. The IR spectra of CO adsorbed on 11.6% Mo/Al_2O_3 are shown in Figure 2. The adsorption of CO on this catalyst at 423 K in the gas phase leads to two overlapping bands at 2112 and 2179 cm^{-1}. The weak peaks at 1626 and 1450 cm^{-1} were observed as well as the CO_2 bands. The intensity of both bands increased when the sample was in the gas-phase CO. The band at 1626 cm^{-1} might be near 1595 cm^{-1} which was characteristic of surface formate. For this case, the bands at 1360 cm^{-1} must also be observed together but there were no peaks around 1360 cm^{-1}. Furthermore, the set of bands in the region of 2840−1980 was not observed for the normal modes of formate species.[9,19] The band at 1450 cm^{-1} would be assigned to the undentate carbonate (asymmetric on CeO_2 at 1460[19,37]), but no peaks were observed near 1350 cm^{-1} (symmetric at 1350−1365 cm^{-1} on NiO,[38] ZnO,[18] and CeO_2[19,37]). As a result, the band at 1450 cm^{-1} corresponds to the negatively charged CO polymers[39] as mentioned for the CO adsorption on the K-promoted $NiMo/Al_2O_3$[9] and MgO (1480 cm^{-1}). The adsorption at 1626 cm^{-1} was the CO band in the stretching vibration mode on the threefold Mo site as will be mentioned later.

CO Adsorption. The interaction of CO with four sites on the β-$Mo_2C(001)$ slab was studied using an orthorhombic supercell. The distance between the carbon atom of CO and the top layer of the Mo slab (ailing *z*-direction) was 2.000 Å before optimization. Four CO-adsorbed models were investigated, corresponding to different adsorption patterns. Figure 3A shows the top and side views of the β-$Mo_2C(001)$ slab before optimization. For model a, CO was placed on the threefold Mo site with the underlying C atom of the second layer of the C atom (a position), that is, the threefold Mo site (Mo1, Mo2, and Mo3) in the top layer. For model b, CO was placed on the threefold Mo site without the underlying C atom (b position), that is, the threefold Mo site, Mo1, Mo3, and Mo4, in the top layer of the Mo atoms. For model c, CO was placed on the twofold Mo site (c position), that is, the twofold position (Mo1 and Mo2) of the top layer of the Mo atoms. For the fourth model (d), the CO was placed on the onefold Mo site (d position), that is, the onefold site (Mo1) in the top layer.

Results of the DFT calculations for the CO adsorption on the four sites (a−d) of the β-$Mo_2C(001)$ slab are illustrated in Figure 3B. The calculated energy changes for the adsorption of CO on the β-$Mo_2C(001)$ slab are listed in Table 1. The adsorption energies for the CO adsorption on the a, b, c, and d

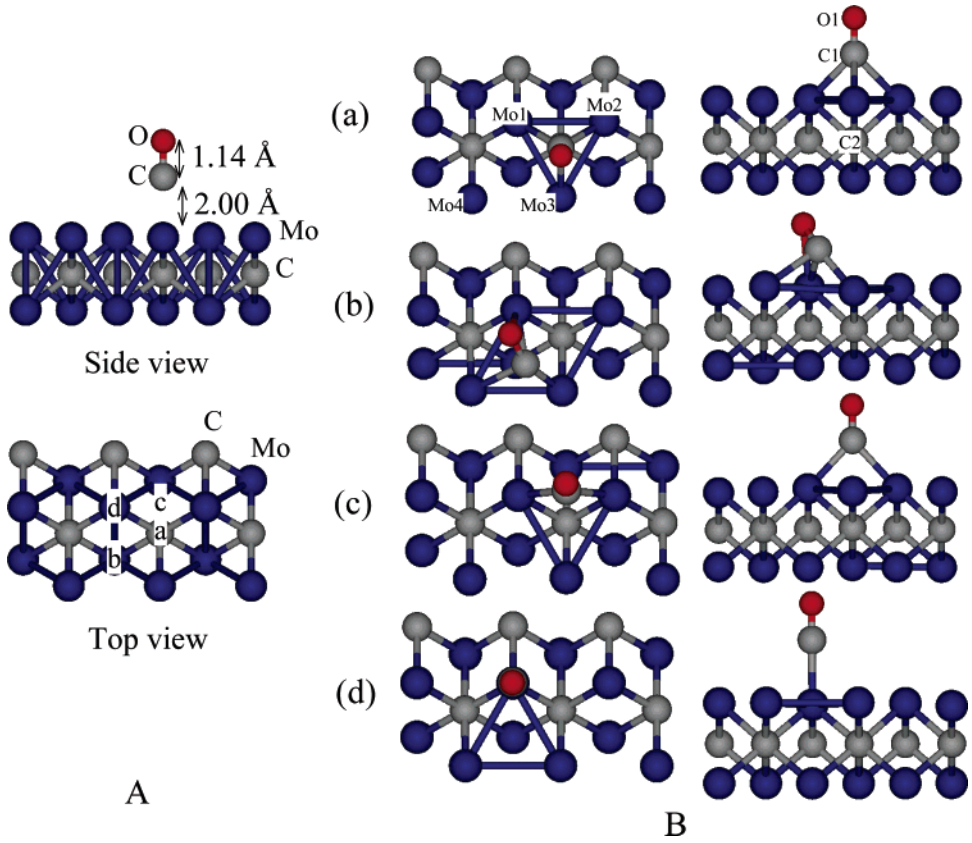

Figure 3. (A) Adsorption structures on the β-$Mo_2C(001)$ slab with side and top views before optimization and (B) a−d adsorbed CO probes with side and top views after optimization.

TABLE 1: Adsorption Energies and Experimental IR Data of CO Adsorption and the Corrected IR Data on the Basis of the IR Peak at 2112 cm^{-1} for the CO Molecule in the Gas Phase

mode	E_{ads}[a](kJ/mol)	ν(CO) (cm^{-1})	corrected[b] ν(CO) (cm^{-1})
CO		2102	2112
CO_2		2319	2330
model a	−281.59	1615	1621
model b	−321.00	1143	1147
model c	−215.24	1645	1652
model d	−160.46	1889	1897

[a] The adsorption energy (E_{ads}) was computed as the difference between the energy of the composite system E(slab + CO) and the sum of the energies of the clean slab E(slab) and uncoordinated adsorbate E(CO): $E_{ads} = E(\text{slab} + \text{CO}) - E(\text{slab}) - E(\text{CO})$. [b] After fitting the calculated and experimental CO stretching vibrations of the free CO molecule, we obtained a scaling factor of 1.0045.

TABLE 2: Bond Lengths of Mo and C of Mo_2C and C−O After CO Adsorption

	bond length (Å)				
		CO adsorption mode[a]			
	CO gas	model a	model b	model c	model d
Mo1−C1		2.28	2.18	2.22	2.10
Mo2−C1		2.28	3.44	2.21	3.65
Mo3−C1		2.27	2.02	3.22	6.63
Mo4−C1		3.80	2.31	4.45	3.62
C1−O1	1.14	1.22	1.36	1.21	1.18

[a] The configurations of a−d are shown in Figure 3.

TABLE 3: Mulliken Charges of Mo Atoms of Mo_2C and C and O Atoms of CO After the Adsorption of CO

			configuration[a]			
	CO gas	$Mo_{12}C_6$ slab	model a	model b	model c	model d
Mo1		3.715	4.480	4.527	4.490	3.886
Mo2		6.027	4.480	4.753	4.502	4.629
Mo3		4.565	4.269	4.039	4.277	4.632
Mo4		5.478	4.496	4.661	4.551	4.626
C2		−2.292	−2.304	−2.286	−2.305	−2.300
C1	0.252		−0.866	−1.114	−0.772	−0.352
O1	−0.098		−0.127	−0.259	−0.113	−0.144

[a] The configurations of a−d are shown in Figure 3.

sites of the β-Mo_2C(001) slab are −281.59, −321.00, −215.24, and −160.46 kJ/mol, respectively. Models a and b have the second and highest adsorption energies, respectively. The bond lengths among the Mo, C, and O atoms with the interaction of the β-Mo_2C and CO after the CO adsorption are shown in Table 2. For model a, the C−O bond length slightly increased from 1.14 Å in the CO gas to 1.22 Å. The bond lengths of the Mo atoms of the slab and C atom of CO, Mo1−C1, Mo2−C1, and Mo3−C1, are 2.28, 2.28, and 2.27 Å, respectively, showing the triangle threefold Mo−C bond for the CO adsorption. The bond length of Mo1−C1 for model a was longer than that for the other models. Furthermore, the mulliken charge of CO before adsorption and the surface Mo atoms of the slab after adsorption are shown in Table 3. For model a, the mulliken charges of the Mo atoms in the top layer were similar but decreased compared to those before the CO adsorption except for the Mo1 atom which became higher. Thus, the electrons transferred from the β-Mo_2C(001) slab to the adsorbed CO. For model b, the lengths of the Mo1−C1, Mo3−C1, and Mo4−C1 bonds were 2.18, 2.02, and 2.31 Å, respectively. The adsorbed CO tilted to the position between the Mo3 and Mo1 atoms with the lowest distance of the Mo3−C1 bond (2.02 Å). In addition, the length of the C−O bond increased to 1.36 Å which was longer than any of the other models. These results indicated the slight cleavage of the C−O bond of CO. The absolute mulliken charges of the C1 and O1 atoms of CO were the highest of all the atoms, leading to a high flow of electrons from the β-Mo_2C(001) slab to the adsorbed CO. Additionally, the adsorption energy for model b was the highest. The larger absolute value of the mulliken charge of the C1 atom of the adsorbed CO corresponds to the greater adsorption energy for the CO adsorption. Concerning the central C atom (C2) in the second layer, the mulliken charge for model b was slightly lower than those for the other slabs (a, c, and d) and those before adsorption, leading to a move of the electrons of the C2 atom to the adsorbed CO and Mo atoms in the top layer. Moreover, for model c, Mo1−C1 and Mo2−C1 had a similar bond length. The bond length of Mo1−C1 for model c was shorter than that for model a. The C−O bond length of CO is 1.21 Å which is similar to that for model a. The Mo1 and Mo2 atoms had similar mulliken charges. For model d, the adsorption energy is the lowest of the four models. The C−O bond length is 1.18 Å and the shortest. The bond length of Mo1−C1 was the shortest. The absolute mulliken charges of the Mo1 and C1 atoms were the lowest of the four models. The mulliken charges of the C1 and O1 atoms of CO were the lowest of the models, producing the lowest flowing electrons from CO to the β-Mo_2C(001) slab.

The IR experimental data, the calculated values from the DFT, and the corrected values are shown in Table 1. The adsorption energy and wavenumber of the CO before and after the optimization for the CO adsorption on β-Mo_2C(001) are also shown. The band at 1626 cm^{-1} was observed, which is quite close to the corrected value of 1621 cm^{-1} for the calculated frequency of the threefold Mo atoms. The IR band at 1626 cm^{-1} in the experiments is the nearest model a at 1621 cm^{-1} and energetically and spectroscopically more stable than model c at 1652 cm^{-1}. This is attributed to the CO adsorption on the threefold Mo atoms. The IR band of model b at the corrected value of 1147 cm^{-1} is far from the observed IR spectra, although model b had the highest adsorption energy. Chen et al.[40] reported that the 1130 cm^{-1} CO species observed in the dissociation can be assigned as bonding both the C and O atoms to the Mo atom of the Mo(110) metal. In fact, the ν(CO) mode at 1147 cm^{-1} can be best described as having the highest adsorption energy but is far from that at the C−O bond of 1626. For model d, the spectrum is different from that of calculated value and model d is the least energetically unstable with the end-on CO coordination. A band near 1450 cm^{-1} was not calculated by the DFT probably due to the negatively charged CO polymers on the alumina. From the IR experiment, the CO adsorption is attributed to model a on the structure of the threefold Mo site with the underlying C atom in the second layer and used for the WGS reaction in the next section. The model b structure will be discussed for CO adsorption on the Mo carbide in the last section.

Selection of Reaction Path Toward $CO + H_2O \rightarrow CO_2 + H_2$ on a β-Mo_2C(001) Slab. Each reaction path during the WGS reaction on the β-Mo_2C(001) slab for model a was calculated and is shown in Figure 4. CO was initially adsorbed on the threefold Mo site (Mo1, Mo2, and Mo3) of model a. H_2O is then set at 2.00 Å over the threefold Mo site. The O2 atom of H_2O was adsorbed on the threefold Mo site lying on the Mo1 atom in the top Mo layer after optimization. CO and H_2O are adsorbed on the β-Mo_2C(001) slab (step 1). In a first step, H_2O can dissociate into OH and H, resulting in configuration b. This result agreed with the data in the references[41,42] (step 2). The optimization of the OH approaching the CO step does not

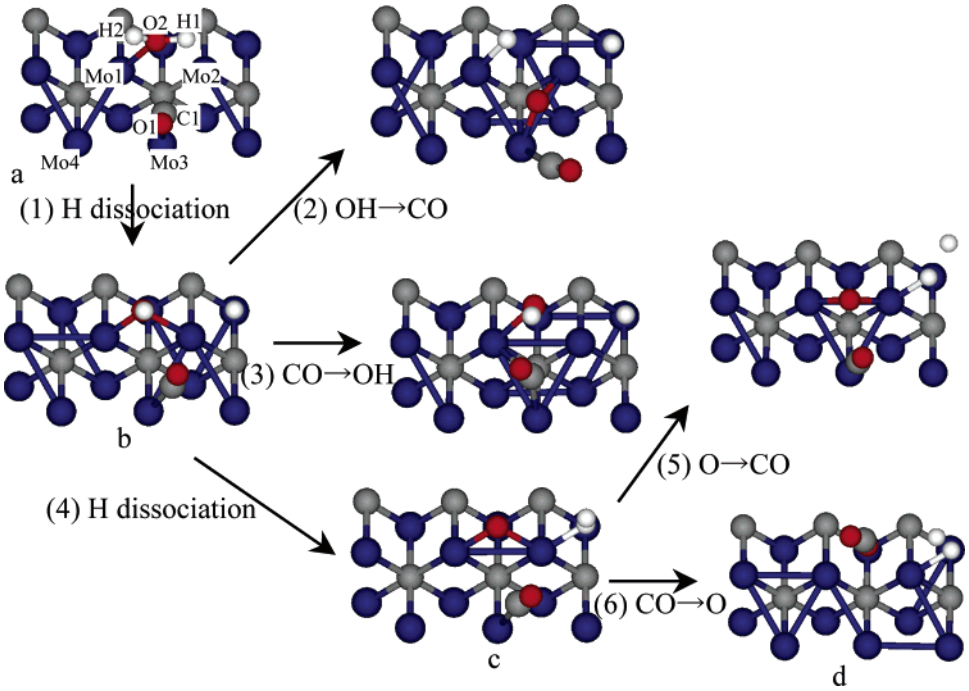

Figure 4. Reaction pathway of the WGS reaction on the β-Mo_2C(001) slab.

produce the formation of CO_2 (step 3). Also, CO approaching OH pulls each other away (step 4). OH is further dissociated into O and H atoms in configuration c (step 5). When the O atom approached CO, each other was pulled away with divergence far from the distance between the H atoms (step 6). Finally, when CO approached O, CO_2 was then formed. As a result, H_2O dissociates into two H atoms and one O atom. The adsorbed CO on the Mo atom approaches the dissociated O atom to form CO_2. This process is related to the second postulated mechanism, the redox process. It is predicted that the redox mechanism is suitable under these experimental conditions. If one assumes a single type of adsorption site, then this mechanism can be written as follows (where * is a free site)

$$CO + * \rightleftarrows CO*$$

$$H_2O + * \rightleftarrows H_2O*$$

$$H_2O* + * \rightleftarrows OH* + H* \qquad \text{(step 1)}$$

$$OH* + * \rightleftarrows O* + H* \qquad \text{(step 4)}$$

$$CO* + O* + 2H* \rightleftarrows CO_2 + H_2 + 4* \qquad \text{(step 6)}$$

It should be noted that the formate is a speculative species only in the WGS reaction on the β-Mo_2C (001) slab and is not involved in this mechanism. Greeley and Mavrikakis used the DFT to suggest that adsorbed OH does not need to further dissociate, at least on Cu catalysts, but could directly react with CO* to form a carboxylate species, COOH*,[43] which then decomposes into H* and CO_2. There is a probability that the adsorbed CO_2 reacted with the adsorbed H and OH to form the formate species (formated reaction, $CO_2* + H* \rightleftarrows HCOO**$). In a previous paper,[44] we reported the hydrogenation of CO_2 on the Mo_4C_2 cluster and found that the activation energy for the hydrogenation of the C atom of CO_2 by the H atom to form HCOO was 119.9 kJ/mol, which was higher by 60.49 kJ/mol than that for the hydrogenation of the O atom to form HO and CO. This result shows that the carbon atom of CO_2 was barely hydrogenated on the Mo_4C_2 cluster and that HCOOH was not produced during the hydrogenation of CO_2 with H_2. Thus, HCOOH was not likely formed on the Mo carbide slab.

We will discuss the possibility of the initial adsorption of H_2O on the β-Mo_2C(001) slab to decompose two H atoms and one O atom which subsequently reacts with the gas-phase CO. The results of the adsorption of H_2O and the subsequent dissociation are shown in Figure 5 and Table 4. The results of the adsorption of H_2O near CO are shown for comparison. In Figure 5, H_2O was set at 2.00 Å over the threefold Mo site of the β-Mo_2C(001) slab using the same procedure as that for model a as shown in Figure 3. After optimization, H_2O was adsorbed at 2.25 Å over the Mo1 position and was located from the initial position at 2.00 Å, although the distance for the coadsorption of CO with H_2O was 1.53 Å in Table 4. The adsorption energy for the H_2O adsorption is 0.021 kJ/mol. This result shows the repulsion of H_2O from the β-Mo_2C(001) slab for the adsorption of H_2O alone without CO adsorption. The distances of Mo1−O and Mo2−O increased, and the O atom of CO was located farther from the Mo1 atom than that for the coadsorption of CO with H_2O. The length of the O−H bonds is close to that of the gas-phase H_2O but shorter than those with the coadsorption. Furthermore, the dissociation of H from H_2O significantly extended the lengths of Mo1−O and Mo2−O to 5.62 and 5.41 Å, respectively, and the height of the O atom from the Mo1 atom became farther apart by 5.20 Å. These values were much higher than the corresponding ones of 2.04, 2.25, and 1.24 Å, respectively, for the coadsorption of CO with H_2O. These results suggest that the OH group is not adsorbed on the β-Mo_2C(001) slab. Thus, H_2O was dissociated in a certain way, $H_2O \rightarrow OH + H \rightarrow O + H + H$, on the β-Mo_2C(001) slab, unless CO was adsorbed near the H_2O adsorption sites. There is little possibility of the first adsorption of H_2O on the β-Mo_2C(001) slab, the decomposition into two H atoms and one oxygen atom, and the subsequent reaction of the oxygen atom with the gas-phase CO.

Energy, Structure, and Mulliken Charge Change in WGS on the β-Mo_2C(001) Slab. Figure 6 shows the energy change diagram of the WGS reaction on β-Mo_2C(001) calculated in terms of the steps calculated for the formation of CO_2, as

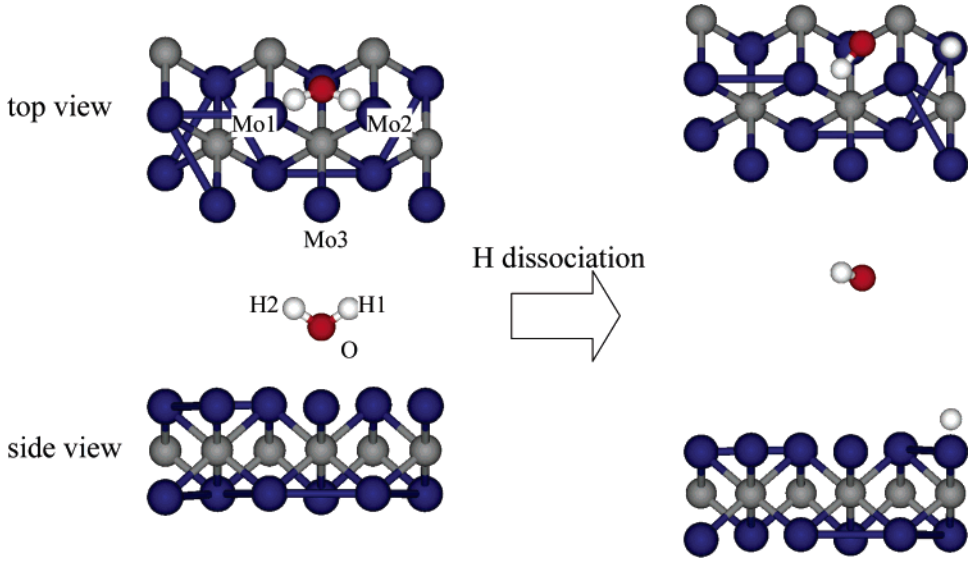

Figure 5. Adsorption of H_2O on the β-Mo_2C(001) slab and the dissociation of H_2O to OH and H.

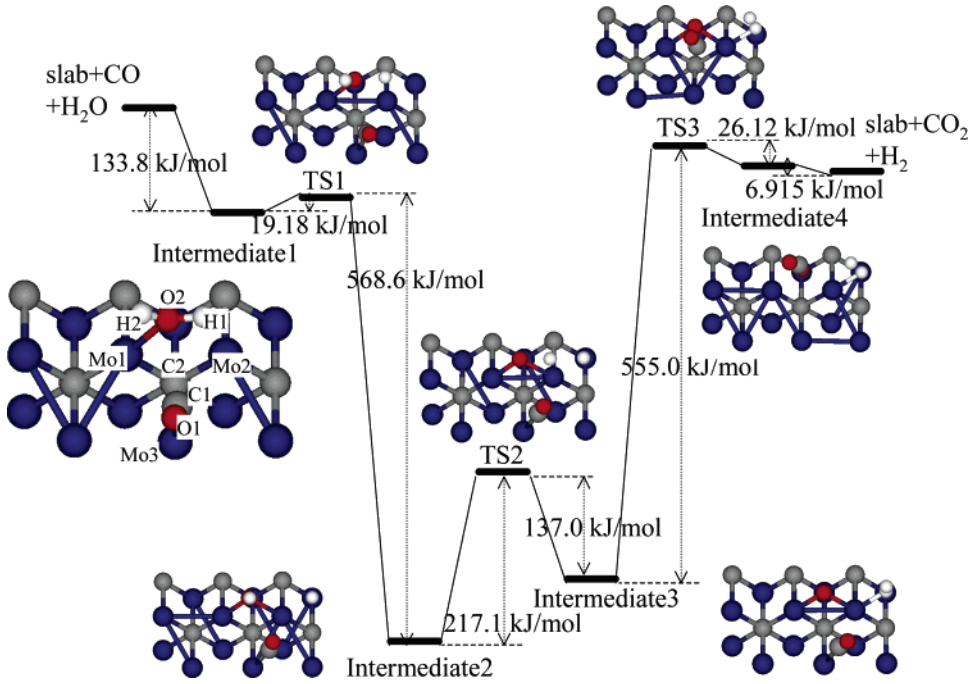

Figure 6. Schematic potential energy surface for the WGS reaction ($CO + H_2O \rightarrow CO_2 + H_2$) on the β-Mo_2C(001) slab.

TABLE 4: Bond Lengths Among the Mo, C, and O Atoms with the Interaction of the β-Mo_2C(001) Slab and H_2O

		H_2O only		adsorbed near CO[a]	
	H_2O gas[b]	H_2O	OH + H	H_2O	OH + H
Mo1−O/Å		2.81	5.62	2.25	2.04
Mo2−O/Å		2.80	5.41	2.58	2.25
O−H1/Å	0.99	1.01	5.04	1.15	3.20
O−H2/Å	0.99	1.01	1.00	1.06	0.99
Mo1−O height/Å		2.25	5.20	1.53	1.24

[a] H_2O adsorbed near CO. [b] One H_2O in the gas phase.

mentioned in the previous section. The activation energy for the reaction process in step 1 of $H_2O \rightarrow H + OH$ (TS1) is 19.18 kJ/mol. This process readily proceeded to intermediate 2 which was the most energetically stable (568.6 kJ/mol). The dissociation in step 4 of OH to form H and O atoms (TS2) is high at 217.1 kJ/mol. The resulting structure (intermediate 3) is unstable after the dissociation of OH into H and O atoms. The final process of the reaction of O with CO to form CO_2 is the high barrier step (555.0 kJ/mol). This step is the rate-determining step (step 6).

The bond lengths of CO and H_2O and the mulliken charges of CO_2, H_2O, and the β-Mo_2C(001) slab during the WGS reaction are shown in Tables 5 and 6, respectively. CO was adsorbed on the threefold Mo site of model a, and H_2O was adsorbed on the threefold Mo site lying on the Mo1 atom of the top Mo layer after optimization. Intermediate 1 shows that the C1 atom of CO is adsorbed on the threefold Mo site by shifting to the Mo3 atom. The bond length of C1−O1 increased from 1.14 Å (CO gas) to 1.19 Å and stayed at 1.17−1.22 Å until desorbing CO_2. The adsorption of H_2O on the threefold Mo position lying on the Mo1 atom shortened the bond length of Mo3−C1 of CO from 2.27 to 2.06 Å and increased those of Mo1−C1 and Mo2−C1 compared to the adsorption of CO alone. The bond lengths of O2−H1 and O2−H2 increased from 0.99 Å (in the gas phase) to 1.15 and 1.06 Å, respectively. This widening of the OH bond length upon the adsorption of H_2O

TABLE 5: Bond Length (Å) of the Mo Atom with C and O of Mo_2C, O−H Bond of H_2O molecule, and C−O Bond of CO

	CO gas	H_2O gas	H_2 gas	int. 1[a]	TS1[b]	int. 2[a]	TS2[b]	int. 3[a]	TS3[b]	int. 4[a]
Mo1−C1				2.75	3.05	3.35	3.33	3.34	3.45	3.56
Mo2−C1				2.72	2.58	2.45	2.56	2.67	3.30	3.63
Mo3−C1				2.06	2.07	2.09	2.13	2.17	3.62	4.88
C1−O1	1.14			1.19	1.21	1.22	1.20	1.18	1.17	1.17
Mo1−O2				2.25	2.16	2.04	2.02	1.98	2.24	2.57
Mo2−O2				2.58	2.40	2.25	2.15	2.03	2.21	2.54
O2−H1		0.99		1.15	1.69	3.20	3.13	3.12	3.17	3.63
O2−H2		0.99		1.06	1.02	0.99	2.09	3.18	2.88	2.52
C1−O2				2.63	2.85	2.84	2.85	2.84	2.04	1.27
H1−H2			0.74	1.88	1.98	3.39	2.47	1.53	1.50	1.47

[a] Int. 1, int. 2, int. 3, and int. 4 are intermediates 1, 2, 3, and 4 in Figure 6, respectively. [b] TS1, TS2, and TS3 are transition states 1, 2, and 3 in Figure 6, respectively.

TABLE 6: Mulliken Charges of Mo and C Atoms of Mo_2C, C and O Atoms of CO, and H and O Atoms of H_2O During the WGS Reaction ($CO + H_2O \rightarrow CO + H_2$)

	H_2O gas	CO_2 gas	int. 1[a]	TS1[b]	int. 2[a]	TS2[b]	int. 3[a]	TS3[b]	int. 4[a]
Mo1			3.770	3.981	4.466	4.681	4.627	4.062	4.237
Mo2			4.573	4.453	4.372	4.459	4.361	3.973	4.329
Mo3			4.660	4.324	4.223	4.123	4.369	4.907	4.114
C2			−2.294	−2.310	−2.312	−2.319	−2.323	−2.319	−2.285
C1		0.621	−0.582	−0.580	−0.745	−0.535	−0.408	0.162	0.588
O1		−0.165	−0.152	−0.127	−0.184	−0.071	−0.078	−0.090	−0.057
O2	−0.495	−0.165	−0.589	−0.716	−0.826	−0.901	−0.962	−0.888	−0.357
H1	0.370		0.069	−0.282	−0.768	−0.769	−0.667	−0.702	−0.693
H2	0.370		0.304	0.390	0.428	−0.222	−0.413	−0.581	−0.488

[a] Int. 1, int. 2, int. 3, and int. 4 are intermediates 1, 2, 3, and 4 in Figure 6, respectively. [b] TS1, TS2, and TS3 are transition states 1, 2, and 3 in Figure 6, respectively.

indicated that the OH bond of H_2O is readily broken into OH (O2−H2) and H1 atoms. The mulliken charge of H1 was extremely decreased at intermediate 1 and then became negative at TS1, leading to the dissociation of the OH group and H^-. Thus, a net charge was transferred from the β-Mo_2C(001) slab to H_2O and CO after adsorption. The step from TS1 to intermediate 2 was the most energetically stable of the reaction. At intermediate 2, the O2 atom bonded to the Mo1 and Mo2 atoms while maintaining the OH (O2H2) bonding. The other H atom (H1) was separated over the threefold Mo site. Meanwhile, the bond length of Mo3−C1 gradually widened from 2.06 Å (intermediate 1) to 2.17 Å (intermediate 3) then suddenly widened to 4.88 Å (intermediate 4). CO_2 left the Mo3 atom of the β-Mo_2C(001) slab. At intermediate 3, the bond length of C1−O2 became shortened from 2.84 Å (intermediate 3) to 1.27 Å to form CO_2 (intermediate 4). Furthermore, the absolute mulliken charge of C1 of the CO molecule reached a maximum at intermediate 2 (OH generation), decreased to intermediate 3, and then became positive at TS3 in the transition state of CO_2 at intermediate 4. The mulliken charge of C1 of the CO turned out to be a positive value, and the electron of O2 inversely returned to the β-Mo_2C(001) slab. The electrons returned at TS3 and intermediate 4 ($O + CO \rightarrow CO_2$). The absolute mulliken charge of the O2 of OH increased from intermediate 1 ($H_2O \rightarrow OH + H$) to intermediate 3 ($O2H2 \rightarrow O2 + H2$) in the dissociation in which O had a negative mulliken charge of H2, but it decreased at TS3 and intermediate 4. This result indicated that the electrons of the β-Mo_2C(001) slab returned to O2H2 and O2 at TS3 and intermediate 4. The step from intermediate 3 to TS3 exhibited a large energy gap for all the steps, that is, the rate-determining step. The TS3 has the highest energy gap for all the steps which are affected by atoms, the positive change in the mulliken charge of the C1 atom and the return to the O2 electrons of the slab. Hwu et al.[41] reported that compared to the Pt and Ru surfaces, the reported results indicated that the carbided W(111) surface had a significantly higher activity toward the dissociation of water. The decomposition of water and surface OH groups are clearly indicated by the production of gas-phase hydrogen for the carbided W(111) surface. Ishikawa et al.[26] reported that H_2O dissociation on pure Pt and on the Pt site in mixed Pt−Ru clusters was difficult by a DFT study. Ru sites more actively dissociated H_2O.[45] In addition, they found that Mo and W were more active toward the H_2O dissociation than Ru.[26] The alloying metals such as Pt−Mo, Pt−W, and Pt−Re were those that possessed low activation energies for the H_2O dissociation and for $CO^* + OH^* \rightarrow COOH^*$ ($+ H^*$) because of its near-zero activation energy for decomposition. Furthermore, the oxidation removal of $CO_{ads(Pt)}$ by $OH_{ads(M)}$ was not as favorable on bimetallic Pt−Mo, Pt−W, Pt−Os, and Pt−Re as on pure Pt, because alloying metals too strongly adsorbed OH. For the (100) surface of TiC, the dissociation of water easily produces hydrogen and hydroxyl groups on the surface and a fully dissociated surface oxide on TiC.[42] At intermediate 4, H1 was adsorbed on the threefold position lying on the Mo2 atom and CO_2 moved over the position between the Mo1 and Mo2 atoms. By H-bonding between the H of H_2O and the O in the reaction of $CO + O + H_2O \rightarrow CO_2 + H_2O$, H_2O would stabilize the TS3 of the reaction and hence reduce the barrier.[25] The approach of the adsorbed H1 to H2 was optimized on the basis of the assumption that the bond length of H−H is 0.74 Å (gas-phase value), but the resulting bond length on intermediate 3 increased to 1.53 Å. H1 and H2 were not molecules. The H1 atom adsorbed on the threefold Mo atom by attracting the Mo2 atom of the β-Mo_2C-(001) slab, but the H2 atom moved over the slab. The O2 atom of H_2O remained bridged by the Mo1 and Mo2. From the result, hydrogen is difficult to be present as a molecule on the β-Mo_2C-(001) slab, as one hydrogen atom was adsorbed and the other was moved. Molecular H_2 would be formed under activation conditions such as high temperature and high pressure. Furthermore, the localized mulliken charge of C2 of the slab was not observably changed during the dissociation of CO and H_2O and the individual reaction ($H + H$ and $CO + O$) during the WGS reaction.

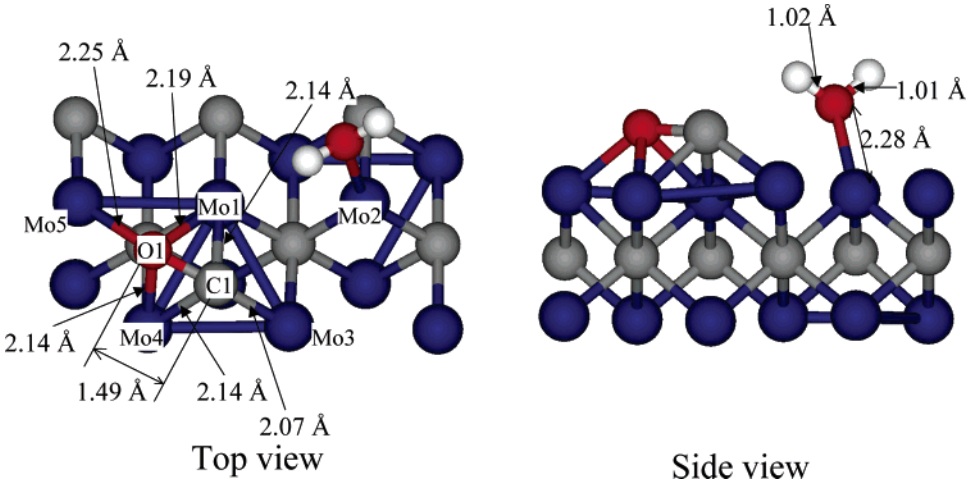

Figure 7. Adsorption of CO in model b upon addition of H_2O on the β-Mo_2C(001) slab—a probability of dissociative adsorption of CO.

Adsorption of H_2O and CO on Model b. As far as model b was concerned, the CO adsorption scheme by the addition of H_2O is shown in Figure 7, because the adsorption energy for the CO adsorption for model b was the highest of all the configurations. The length of the C−O bond increased to 1.49 from 1.36 Å after optimization (1.14 Å in CO gas). The distances of the Mo−C bond (Mo1, Mo3, and Mo4) were 2.14, 2.07, and 2.14 Å, respectively, and those of the Mo−O bond (Mo1, Mo4, and Mo5) were 2.19, 2.14, and 2.25 Å, respectively. These values corresponded to the near position of the threefold Mo site on the top layer. In model b, CO was slightly dissociated (Figure 3) for CO adsorption alone. When the adsorption of H_2O on the site near the adsorbed CO on the β-Mo_2C(001) slab occurred, CO would be dissociated. This calculation indicates that the H_2O induction on the β-Mo_2C surface dissociated CO into C and O atoms. It is suggested that the procedure under severe reaction conditions such as high temperature and CO high pressure probably enhances the CO dissociation. Thus, the adsorption structure, model b, is expected to be the intermediate step for the dissociation of the CO molecule.

Conclusion

The periodic, self-consistent, gradient-corrected DFT of the WGS reaction on the β-Mo_2C(001) slab was performed. This reaction pathway involved the adsorption of CO, the decomposition of H_2O, and the subsequent reaction of the decomposed H_2O with CO. The IR spectra of the CO adsorption was experimentally studied for the identification of several possible adsorption modes of CO. The DFT calculated the adsorption of CO on threefold Mo sites in the top layer with (a) and without (b) the underlying C atom, (c) the twofold Mo site, and (d) the onefold Mo site. The IR band at 1626 cm^{-1} for the CO adsorption corresponded to that at a. The adsorption energies for the CO adsorption on a, b, c, and d were −281.59, −321.00, −215.24, and −160.46 kJ/mol, respectively. The large absolute value of the mulliken charge of the C atom of the adsorbed CO is related to the greater adsorption energy. The C−O bond length increased from 1.36 to 1.49 Å after the H_2O adsorption b, suggesting the dissociation of C−O after the CO adsorption of CO and H_2O. The calculated reaction for WGS proceeded as follows. (1) In the first step, H_2O dissociates into OH and H. (2) The optimization of the approaching OH to CO step does not produce the formation of CO_2 but the dissociation of OH into O and H. (3) The OH is further dissociated into O and H atoms. (4) CO approached O in which the step exhibited a large energy gap in all the steps, that is, the rate-determining step. CO_2 is then formed.

Acknowledgment. This study was carried out as a research project funded by a Grant-In-Aid for Scientific Research from the Ministry of Education, Culture, Sports, Science and Technology, Japan.

References and Notes

(1) Li, Y.; Du, Q.; Flytzani-Stephanopoulos, M. *Appl. Catal., B* **2000**, *27*, 179.
(2) Tanaka, Y.; Utaka, T.; Kikuchi, R.; Sasaki, K.; Eguchi, K. *Appl. Catal., A* **2003**, *242*, 287.
(3) Rhodes, C.; Hutchings, G. J.; Ward, A. W. *Catal. Today* **1995**, *23*, 43.
(4) Van Herwijnen, T.; De Jong, W. A. *J. Catal.* **1980**, *63*, 83.
(5) Ovesen, C. V.; Clausen, B. S.; Hammershoei, B. S.; Steffensen, G.; Askgaard, T.; Chorkendorff, I.; Nørskov, J. K.; Rasmussen, P. B.; Stoltze, P.; Tayer, P. *J. Catal.* **1996**, *158*, 170.
(6) Campbell, C. T.; Daube, K. A. *J. Catal.* **1987**, *104*, 109.
(7) Ghenciu, A. F. *Curr. Opin. Solid State Mater. Sci.* **2002**, *6*, 389.
(8) Ladebeck, J. R.; Wagner, J. P. In *Handbook of Fuel Cell Technology-Fundamentals, Technology, and Applications*; Vielstich, W., et al. Eds.; Wiley: 2003; Chapter 17.
(9) Kantschewa, M.; Delannay, F.; Jeziorowski, H.; Delgado, E.; Eder, S.; Ertl, G. *J. Catal.* **1984**, *87*, 482.
(10) Michal, A.; Henkel, H. J.; Koch, C.; Kostka, H. German Patent. 2, 643, 916, 1978.
(11) Segura, M. A.; Aldridge, C. L.; Riley, K. L.; Pine, L. A. U.S. Patent, 4054644, 1997.
(12) Kettmann, V.; Balgavý, P.; Sokol, L. *J. Catal.* **1988**, *112*, 93.
(13) Nickolov, R. N.; Edreva-Kardjieva, R. M.; Kafedjiysky, V. J.; Kikolova, D. A.; Stankova, N. B.; Mehandjiev, D. R. *Appl. Catal., A* **2000**, *190*, 191.
(14) Hou. P.; Meeker, D.; Wise, H. *J. Catal.* **1983**, *80*, 280.
(15) Łaniecki, M.; Małecka-Grycz, M.; Domka, F. *Appl. Catal., A* **2000**, *196*, 293.
(16) Patt, J.; Moon, D. J.; Phillips, C.; Thompson, L. *Catal. Lett.* **2000**, *65*, 193.
(17) Moon, D. J.; Ryu, J. W. *Catal. Lett.* **2004**, *92*, 17.
(18) Shido, T.; Iwasawa, Y. J. *Catalysis* **1991**, *129*, 343.
(19) Shido, T.; Iwasawa, Y. J. *Catalysis* **1993**, *141*, 71.
(20) Grenoble, D. C.; Estadt, M. M.; Ollis, D. F. J. *Catalysis* **1981**, *67*, 90.
(21) Ovesen, C. V.; Stoltze, P.; Nørskov, J. K.; Campbell, C. T. J. *Catalysis* **1992**, *134*, 445.
(22) Koryabkina, N. A.; Phatak, A. A.; Ruettinger, W. F.; Farranto, R. J.; Ribeiro, F. H. J. *Catalysis* **2003**, *217*, 233.
(23) Campbell, J. M.; Nakamura, J.; Campbell, C. T. J. *Catalysis* **1992**, *136*, 24.
(24) Jiang, L.; Wang, G.-C.; Cai, Z.-S.; Pan, Y.-M.; Zhao, X.-Z. *J. Mol. Structure. (THEOCHEM)* **2004**, 710, 97.
(25) Gong, X.-Q.; Hu, P. *J. Chem. Phys.* **2003**, *119*, 6324.
(26) Ishikawa, Y.; Liao, M.-S.; Cabrera, C. R. *Surf. Sci.* **2002**, *513*, 98.
(27) Hou, H.; Muckerman, J. T.; Liu, P.; Rodriguez, J. A. *J. Phys. Chem. A* **2003**, *107*, 9344.

(28) Liu, P.; Rodriguez, J. A. *J. Chem. Phys.* **2004**, *120*, 5414.
(29) Liu, P.; Rodriguez, J. A. *Catal. Lett.* **2003**, *91*, 247.
(30) Travert, A.; Dujardin, C.; Maugé, F.; Cristol, S.; Paul, J. F.; Payen, E.; Bougeard, D. *Catal. Today* **2001**, *70*, 255.
(31) Zeng, T.; Wen. X.-D.; Wu. G.-S.; Li, Y.-W.; Jiao, H. *J. Phys. Chem. B* **2005**, *109*, 2846.
(32) Liu, P.; Rodriguez, J. A.; Asakura, T.; Gomes, J.; Nakamura, K. *J. Phys. Chem. B* **2005**, *109*, 4575.
(33) CPMD, copyright IBM Corp., 1990−2001, copyright MPI für Festkörperforschung Stuttgart, 1997−2005.
(34) Perdew, J. P.; Burke, K.; Ernzerhof, M. *Phys. Rev. Lett.* **1996**, *77*, 3865.
(35) Fuchs, M.; Scheffler, M. *Comput. Phys. Commun.* **1999**, *119*, 67.
(36) *CRC Handbook of Chemistry and Physics*, 81st ed.; Lide, D. R., Ed.; CRC Press: Boca Raton, FL, 2000.
(37) Jacobs, G.; Patterson, P. M.; Graham, U. M.; Sporks, D. E.; Davis, B. H. *Appl. Catal., A* **2004**, *269*, 63.
(38) Matsumoto, T.; Bandara, A.; Kubota, J.; Hirose, C.; Domen, K. *J. Phys. Chem. B* **1998**, *102*, 2979.
(39) Coluccia, S.; Garrone, E.; Guglielminotti, E.; Zecchina, A. *J. Chem. Soc., Faraday Trans. 1* **1981**, *77*, 1063.
(40) Chen, J. G.; Colaianni, M. L.; Weinberg, W. H.; Yates, J. T., Jr. *Chem. Phys. Lett.* **1991**, *177*, 113.
(41) Hwu, H.; Polizzotti, B. D.; Chen, J. G. *J. Phys. Chem. B* **2001**, *105*, 10045.
(42) Didziulis, S. V.; Frantz, P.; Perry, S. S.; El-bjeirami, O.; Imaduddin, S.; Merrill, P. B. *J. Phys. Chem. B* **1999**, *103*, 11129.
(43) Greely, J.; Mavrikakis, M. *J. Catal.* **2002**, *208*, 291.
(44) Tominaga, H.; Nagai, M. *Appl. Catal., A* **2005**, *282*, 5.
(45) Liao, M.-S.; Cabrera, C. R.; Ishikawa, Y. *Surf. Sci.* **2000**, *445*, 267.